THE JOURNAL OF PHYSICAL CHEMISTRY C

ARTICLE

pubs.acs.org/JPCC

Effects of Periodic Illumination and Aqueous/Organic Interfacial Surface Area on Chain Propagation of CCl_3F Reduction

Kurt Winkelmann,[*,†] Robert L. Calhoun,[‡,§] and G. Mills[*,‡]

[†]Department of Chemistry, Florida Institute of Technology, Melbourne, Florida 32901, United States

[‡]Department of Chemistry and Biochemistry, Auburn University, Auburn, Alabama 36849, United States

ABSTRACT: Periodic illumination and changes in the interfacial aqueous-CFC surface area reveal interesting features of the propagation process occurring during the photoinitiated chain reduction of trichlorofluoromethane (CFC 11) to $CHCl_2F$ and Cl^- in TiO_2 suspensions containing HCO_2^- ions. Formate ions serve as hole scavengers on the TiO_2 surface and react with $\bullet CCl_2F$ radicals to form $HCCl_2F$ and $\bullet CO_2^-$. Carboxyl radicals are capable of propagating the chain reaction in the solution phase by reducing CCl_3F. Chain reduction of CCl_3F continues after illumination has ceased, and the postirradiation reactions constitute 10% or more of the total Cl^- yield. The dark reduction of CFC 11 provides further support to the proposed mechanism in which $\bullet CCl_2F$ and $\bullet CO_2^-$ ions function as chain carriers. The reaction rate measured during a period of illumination is affected by the length of the preceding dark period. In addition, the rate of CCl_3F reduction is significantly enhanced by the presence of excess CFC 11, which forms a second, nonaqueous liquid phase. The CCl_3F liquid phase in the aqueous, UV irradiated TiO_2 suspension increases the photonic efficiency of the reaction by a factor of 4 in both degassed and air saturated systems. Postirradiation reactions occur only in the presence of excess CFC liquid. Kinetic effects of a second liquid phase are a consequence of propagation steps occurring at the water−CCl_3F interface with moderately rapid transfer of reactants across the phase boundary. Factors that increase the total surface area of that boundary, such as smaller droplets or greater volume of CCl_3F liquid, lead to higher photonic efficiencies.

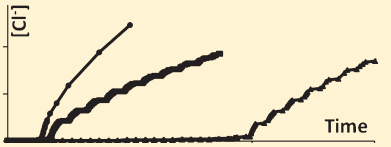

INTRODUCTION

Chemical reactions can be initiated on the surface of semiconducting titanium dioxide particles suspended in solution by the absorption of ultraviolet light.[1,2] Photogenerated conduction band electrons (e^-_{cb}) and valence band holes (h^+_{vb}) become delocalized within the semiconductor. These charge carriers either recombine releasing heat or migrate to the TiO_2 surface where they can form radicals, such as •OH species.[3] Generation of reactive radicals via photolysis of air saturated aqueous TiO_2 suspensions have been frequently used to degrade pollutants. For instance, oxidation of organic chemicals can be induced by h^+_{vb} and/or •OH, while another species, often O_2, prevents charge carrier recombination by scavenging e^-_{cb}.[1,2] Multiple intermediates can form given that several reaction channels are available. The intermediates continue to decay through additional steps that lower the efficiency of the degradation process, particularly if additional e^-_{cb} or h^+_{vb}/•OH are consumed. Phototransformation of fully halogenated alkanes in TiO_2 suspensions is even less efficient since these chemicals are not susceptible to oxidation.

However, reductive dehalogenation of fully halogenated alkanes appears to provide a chemical pathway for their degradation in oxygen-free natural systems.[4] Faster dehalogenations occur through radical chain reactions.[5] Particularly effective transformations take place when the carboxyl radical anion ($\bullet CO_2^-$) is a chain carrier due to the strong reducing nature of this species, $E°(CO_2/\bullet CO_2^-) = -1.8$ V.[6] Because •OH reacts with HCO_2^- to form $\bullet CO_2^-$, efficient chain reductive dechlorinations seemed feasible upon illumination of air-free TiO_2 suspensions in the presence of formate ions. Chlorofluorocarbons (CFCs) were selected to test this strategy given that these compounds are inert toward oxidative degradation, a property that plays an important role in their disruptive effect on the stratospheric ozone cycle.[7] In addition, $\bullet CO_2^-$ is known to induce selective reduction of CFCs into their hydrogen-substituted analogues (HCFCs),[5b] which serve as replacements of chlorofluorocarbons in view of their susceptibility to oxidative decay.[8] Investigations with CCl_2FCF_2Cl (CFC 113) and CCl_3CF_3 (CFC 113a) provided evidence that the photoreductions formed mainly the corresponding HCFCs via radical chain reactions.[9] Subsequent experiments with CCl_3F (CFC 11) yielded dechlorinations with higher efficiencies even in suspensions initially containing air, where long chains ensued after an induction period corresponding to the O_2 reduction.[10] The fast photochemical dehalogenations of CCl_4 observed in basic TiO_2 suspensions containing alcohols as h^+_{vb}/•OH scavengers have also been interpreted in terms of chain processes.[11]

Kinetic information gathered during the chain photoreduction of CFC 11 was consistent with solution processes that were not influenced by binding equilibrium of formate ions (the h^+_{vb} /•OH scavengers) on the oxide surface.[10] Similar conclusions were reached in studies on the HCO_2^- oxidation using intermittent photolysis techniques.[12] As is typical in photoreactions involving TiO_2, recombination of charge carriers inside the semiconductor limited initiation of the CFC 11 photoreduction. Charge carrier recombination is sensitive to changes in the reactivity of e^-_{cb}

Received: June 13, 2011
Revised: December 22, 2011
Published: December 23, 2011

(the weakest reductant) as a function of pH,[13] and also to electron trapping in the oxide lattice.[14] In fact, conversion of e^-_{cb} into the stronger reductant $\bullet CO_2^-$ drastically improved the efficiency of the photodehalogenation.[10] High CFC volumes and $[HCO_2^-]$ were employed because both chemicals are involved in the propagation steps. Such reaction conditions enabled chains to propagate away from the oxide surface, thereby suppressing multiple scavenging of charge carriers. These conditions also favored generation of the desired HCFC product through fast propagations with minimal interference from termination steps. Given the limited solubility of CCl_3F in water of 8.1 mM,[15] excess liquid CFC was introduced in the TiO_2 suspensions in order to maintain a constant aqueous $[CCl_3F]$ throughout the photoreactions. Subsequent results from experiments involving periodic illuminations are presented here, which reveal interesting features of the chain reactions. In addition, evidence is presented that the excess CFC affects both the photochemical and postirradiation reactions.

EXPERIMENTAL METHODS

All chemicals were used as received from Fisher or Aldrich unless otherwise noted. Water used in solutions was deionized using a Milli-Q-Plus system (Millipore, $\rho > 18$ MΩ). Titanium dioxide powder (Degussa P25, average 30 nm diameter particles) was used as the sensitizer dispersed in 110.0 mL of aqueous solutions containing sodium formate/formic acid buffers. Suspensions containing 0.50 g L^{-1} of TiO_2 were employed given that the highest rates of CFC photoreduction were achieved with such an amount of oxide powder.[9] Most experiments were conducted at pH 5.9 with a total concentration of the formic acid/formate buffer equal to 0.300 M. At this pH, the buffer concentration is often represented here by $[HCO_2^-]$ since formate ions are the predominant species. For reactions involving different pH values, the ratio of HCO_2^-/HCO_2H was varied while maintaining a total buffer concentration of 0.300 M. Illuminations were typically performed with suspensions containing 2.0 mL of liquid CCl_3F, except for experiments that explored the dependence of reaction rate on volume of CFC 11 added. In most cases, the added CFC volumes exceeded the solubility limit (82 μL in 110.0 mL of suspension), resulting in a second, denser CCl_3F phase saturated with H_2O ($d(CCl_3F) = 1.47$ g cm^{-3}).[15] Stirring the mixture dispersed the CFC liquid into small, spherical droplets within the aqueous phase. When appropriate, a digital stirring plate (Thermix 120 MR) was used to quantify the effect of stirring rate on the photoreaction.

Procedures and equipment used for photochemical experiments have been described previously.[10] The photochemical reactor consisted of a double-walled glass vessel with an internal volume of 170 mL that was tightly sealed with Suba Seal rubber septa. *Caution should be exercised when performing similar experiments because sealed reactor vessels have shattered occasionally due to excessive pressure generated by the production of gas phase products during irradiation.* Suspensions free of air were prepared by bubbling them for 30 min with Ar under stirring prior to the addition of the CFC in order to avoid evaporation of CCl_3F (bp = 23.8 °C).[15] Liquid trichlorofluoromethane was degassed using a freeze−pump−thaw method three times and injected into the sealed reactor vessel via gastight syringes. Each illumination was preceded by a dark equilibration time during which the suspension was stirred for 15 min. Kinetic data collected during irradiation were independent of the equilibration time beyond 15 min. Chloride and fluoride ion selective electrodes (ISE) monitored ion concentrations in situ, while the suspension was irradiated and stirred. Electrodes were calibrated in the dark using solutions identical to those used in the photochemical reactions. Because of the configuration of the reaction vessel, only one ISE could be used for a given experiment. Most experiments were performed at least twice with typical deviations of less than 20%.

Illuminations employed a PTI 1010 S system described before;[10] light was passed through filters (water and a Kopp GS-7-60) to select 320−385 nm photons with a transmittance maximum at 360 nm. Determination of the incident light intensity (I_o, $1-1.1 \times 10^{-6}$ M ($h\nu$) s^{-1}) was performed with the Aberchrome 540 actinometer.[16] The photodehalogenation effectiveness was characterized using the photonic efficiency (P.E.), which corresponds to the rate of product formation divided by the intensity of incident photons. Hence, P.E. values are lower limits of the quantum yields and were obtained using reaction rates measured during a time span of at least 40 s of linear increase in product concentration. Some procedures are available for determining the intensity of light scattered by TiO_2 particles, which aid determination of quantum yields.[17] However, these methods do not account for photons scattered by the CFC droplets and were, therefore, not employed in this study. Post irradiation effects were studied by blocking the path of the light beam or turning off the lamp.

RESULTS

Detailed accounts of the photodehalogenation of CCl_3F in the presence of formate ions have been presented elsewhere[10] but are summarized here to allow straightforward comparisons to the recently collected data. Chloride ions and dichlorofluoromethane ($CHCl_2F$) are the primary products formed during UV irradiation of an aqueous TiO_2 suspension containing formate ions and CCl_3F liquid. The presence of ambient light has no effect on the reaction. Upon exposure to UV light, Cl^- forms slowly during an induction period that varies from <3 min for degassed systems to approximately 15 min for air saturated suspensions. Following the induction period, the rate of chloride production, $r(Cl^-)$, increases suddenly and then gradually declines under continued illumination. The maximum initial rate of chloride ion formation, $r(Cl^-)_i$, was determined during the period of fast $[Cl^-]$ increase occurring at the beginning of the second stage and was used to calculate initial photonic efficiency values ($P.E.(Cl^-)_i$). Almost 99% of the total amount of Cl^- forms after the induction period is complete. At pH = 5.9, air-free systems yield $P.E.(Cl^-)_i$ values equal to 7.9 and the concentration of chloride ions after 60 min of illumination is 5 mM. For air-saturated systems, $P.E.(Cl^-)_i = 15$ and $[Cl^-]$ after 60 min of illumination is 20 mM. The large photonic efficiencies indicate that the photoreduction of CFC 11 proceeds via chain processes even in systems initially containing air. Illuminations carried out in the absence of HCO_2H/HCO_2^- yielded negligible amounts of Cl^- ions, demonstrating that the formate species interfere with the recombination of photogenerated charge carriers.[18]

In this study, additional experiments have been performed to evaluate the effect of periodic illumination on the photoreduction of CCl_3F in UV-irradiated TiO_2 suspensions. Blocking the incident light with an opaque board and turning off the lamp has the same effect. Compared in Figure 1 are Cl^- generation data obtained when air-saturated suspensions at pH = 5.9 were treated with different illumination conditions. Curve A resulted upon

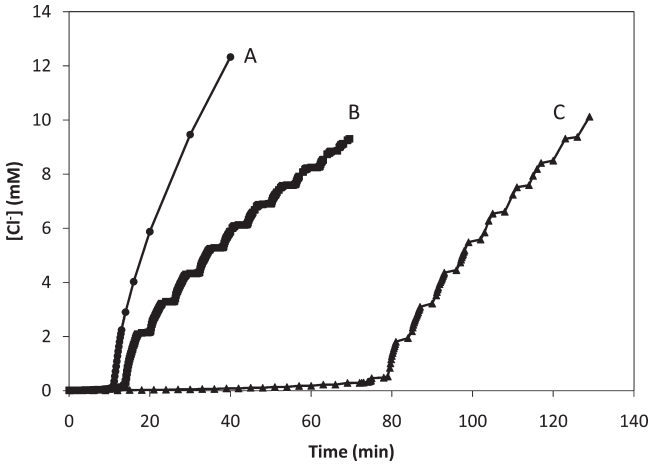

Figure 1. Formation of Cl^- over time for aerated suspensions under different illumination conditions: continuous light exposure (curve A, ●), 3 min light/3 min dark cycles beginning after induction period is complete (curve B, ■), and 3 min light/3 min dark cycles throughout reaction (curve C, ▲). All suspensions contained 0.3 M formate/formic acid buffer, 0.50 g L^{-1} of TiO_2, and 2.0 mL of CCl_3F at pH 5.9 and were irradiated with $I_o = 1.0 \times 10^{-6}$ M $h\nu$ s^{-1}.

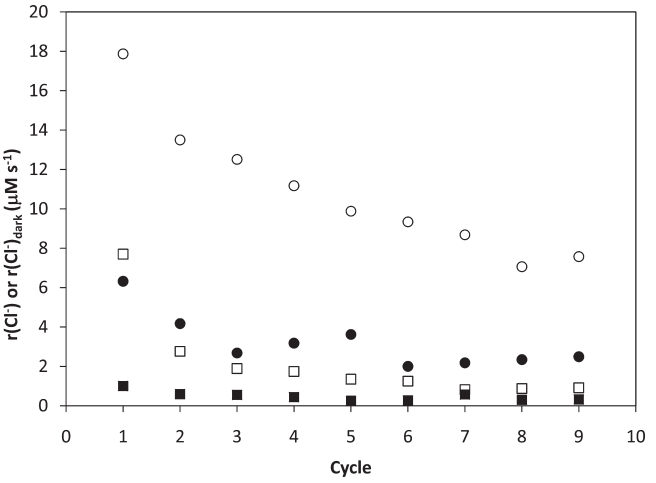

Figure 2. Rate of Cl^- formation for air-saturated suspensions measured during cycles consisting of a 3 min illumination period (○) and in the dark for 3 min after photolysis (●), as well as for air-free suspensions while illuminated (□) and during the dark period (■). All suspensions contained 0.3 M formate/formic acid buffer, 0.50 g L^{-1} of TiO_2, and 2.0 mL of CCl_3F at = pH 5.9 and were irradiated with $I_o = 1.0 \times 10^{-6}$ M $h\nu$ s^{-1}.

continuous illumination, whereas the data of curve B was acquired via uninterrupted photolysis during the induction period, followed by alternating 3 min periods of light and 3 min periods of dark. In both cases, the cumulative irradiation time was 30 min, and the lengths of induction periods (11 and 14 min) are typical for air-saturated suspensions under continuous irradiation. The data shows that $r(Cl^-)_i$ was very similar in both experiments, and curve B provides evidence that Cl^- ions continued to be formed after illumination was interrupted. Postirradiation effects are typical of free radical processes taking place via long chain reactions, such as during the radiolytic CCl_4 reduction in the presence of H-atom donors.[19] Thus, the results presented in Figure 1 provide further support to the interpretation that the CCl_3F photoreduction initiated by TiO_2 occurs via a chain process.[10]

Curve C of Figure 1 shows data gathered by exposing a suspension to alternating 3 min periods of light and dark during the entire reaction, including the induction period. In this case, a much longer induction period of 78 min was observed, and the fast step of Cl^- generation was not detected until the cumulative time of light exposure amounted to 39 min. Formation of chloride was detected only during the illumination periods of the long induction step showed in curve C and not during the dark periods. Thus, the O_2 molecules remaining in the suspension scavenge the photogenerated reducing radicals and inhibit quickly the CCl_3F reduction initiated in the presence of light. In general, the amounts of products formed during the induction periods were insignificant as compared to the yields typical of the second, faster phase of the CCl_3F reduction. Also, none of the kinetic data of Figure 1 obtained during the induction periods followed a simple rate law. These results agree with prior observations and suggest that the dominant process taking place during the induction period is not a chain transformation best described by the overall reaction[10]

$$CCl_3F + 4e^- + 4H^+ + O_2 \rightarrow CO_2 + 3HCl + HF \quad (1)$$

Therefore, data analysis was centered on the results obtained during the second stage of the CCl_3F photoreduction.

Each curve of Figure 1 includes data collected for a total of 30 min of illumination after the initial induction period. The final chloride ion concentrations of these experiments (9.5−12.5 mM) were within the range of those obtained via continuous photolysis of air-saturated suspensions for the same amount of time.[10a] In both experiments that yielded curves B and C, chloride ions continued to form after illumination was interrupted. However, the postirradiation process was significantly slower than the Cl^- generation under illumination and took place only during the first 90 s of the 3 min dark period. Also, the amount of Cl^- formed in the postirradiation process decreased during each subsequent dark period. For instance, 0.22 mM Cl^- formed during the first dark period, whereas only 0.06 mM halide ions resulted from the eleventh and last dark period. The cumulative amount of chloride ions formed during the dark periods in curves B and C of Figure 1 was 0.90 ± 0.25 mM and constitutes 10% of their total Cl^- yield. In addition, short induction periods, lasting 45−60 s, occurred at the beginning of each 3 min exposure that followed a dark period. Rapid chloride ion formation began after this brief delay.

Postirradiation reactions were also observed in suspensions degassed prior to irradiation (data not shown). Since the induction period of argon-saturated suspensions amounted to 0.5−2 min, these systems were exposed to 3 min of light followed by dark periods of equal length throughout the experiments. Slow postirradiation reactions ensued, but unlike the equivalent processes detected in air-saturated suspensions, formation of Cl^- was continuous during the entire dark periods. As a result, the cumulative amount of generated Cl^- (0.82 mM) during the dark periods was approximately equal to the postirradiation yield of chloride ions of air-saturated suspensions. Analogous to the later systems, the increase in $[Cl^-]$ became smaller with each subsequent dark period. However, no induction period was observed when photolysis was restarted, which induced an instantaneous increase in the rate of chloride ion formation. Similar light/dark cyclic experiments were performed with air-free suspensions at pH = 4 and pH = 8. These experiments showed that Cl^- was generated in a manner similar to continuously irradiated suspensions.[10b] For example,

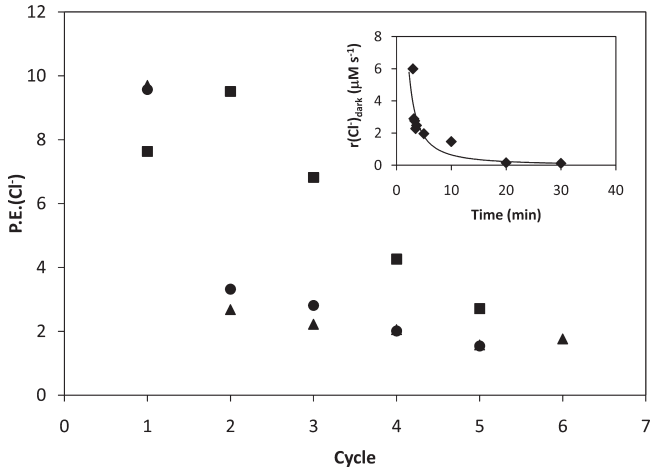

Figure 3. P.E.(Cl^-) as a function of cycle with 3 min of light exposure followed by dark periods lasting 27 min (■), 17 min (●), or 30 s (▲). All deaerated suspensions contained 0.50 g L^{-1} of TiO_2, 0.3 M formate/formic acid buffer at pH 5.9, and 2.0 mL of CCl_3F and were irradiated with $I_o = 1.0 \times 10^{-6}$ M $h\nu$ s^{-1}. Inset shows the decline of $r(Cl^-)_{dark}$ for an Ar-saturated suspension as a function of time after a 3 min period of illumination.

at pH = 8 the rate of chloride photogeneration, $r(Cl^-)$, decreased as the number of illumination steps increased, and the formation rate in the dark, $r(Cl^-)_{dark}$, followed the same trend. However, $r(Cl^-)$ increased with each subsequent illumination step at pH = 4, which was also the case for $r(Cl^-)_{dark}$. The consequence of this behavior was that the cumulative concentration change derived from the dark reactions amounted to 0.8 mM Cl^- regardless of pH.

Compared in Figure 2 are the reaction rates determined during photolysis and dark periods for suspensions initially saturated with air or Ar. The rates are presented as a function of the number of duty cycles, where each cycle consisted of a 3 min light exposure and a dark period of the same length. Analogous to the case of the experiment of curve B in Figure 1, all air-containing suspensions were irradiated continuously during the induction periods. Periodic photolysis/dark cycles began once these processes were completed. As mentioned before, air-saturated suspensions exhibited by a brief period of negligible Cl^- formation occurring at the beginning of each photolysis step. Thus, maximum $r(Cl^-)$ values were determined immediately after such periods. Figure 2 shows that for both systems $r(Cl^-)$ and $r(Cl^-)_{dark}$ gradually declined with increasing number of cycles throughout the experiments. In all cases, $r(Cl^-)_{dark}$ values were lower (by factors between 3 and 10) than those determined for the preceding and also subsequent photolysis periods. Except for the first cycle, where the rate ratio was about 2, air-saturated suspensions exhibited $r(Cl^-)$ values between 8 to 10 times higher than the rates obtained in the absence of air. Formation rates in the dark followed a similar trend, but the difference between $r(Cl^-)_{dark}$ values decreased with increasing number of cycles. Measurements of fluoride ion concentration during postirradiation experiments demonstrated that $[F^-]$ and $r(F^-)$ behaved in a way analogous to the chloride ion data. However, the resulting $[Cl^-]$ was always much greater than $[F^-]$ and the ratios of $r(Cl^-)$ to $r(F^-)$ remained above 100 during light and dark periods. These findings are in good agreement with the ratios of concentrations and rates determined under continuous illumination.[10]

Depicted in Figure 3 is the evolution of photonic efficiencies with increasing number of cycles for air-free suspensions. Three series of experiments were conducted keeping a constant exposure time of 3 min but using dark periods of different lengths: 30 s (▲), 17 min (●), and 27 min (■). The photonic efficiencies correspond to the maximum $r(Cl^-)/I_o$ values measured during the photolytic period of each cycle. Because of the variable length of the induction period, the maximum $r(Cl^-)$ for cycle 1 was determined within the first 3 min of irradiation, whereas rate maxima were always noticed during the first 40 s of each subsequent cycle. Comparison of the results from Figure 3 with those obtained using dark periods of 3 min, labeled with □ in Figure 2, indicate that the P.E.(Cl^-) evolution remained unaffected when the length of the preceding dark period varied between 0.5 and 17 min. P.E.(Cl^-) declined significantly in all these experiments after the first three minutes of irradiation (cycle 1) and continued to slowly decrease after each subsequent cycle. Obviously, dark periods lasting up to 17 min had no effect on the rate of chloride ion formation obtained during the subsequent illumination period. Furthermore, the P.E.(Cl^-) values obtained at the beginning of each cycle were close to the instantaneous photonic efficiencies determined for suspensions continuously irradiated for the same total length of time. In contrast, the high initial P.E.(Cl^-) value was maintained for 2 cycles, and a less pronounced subsequent decline in photonic efficiency was noticed when the dark periods amounted to 27 min. The inset of Figure 3 shows the variation of the instantaneous $r(Cl^-)$ as a function of time determined during a postirradiation process initiated by a single 3 min illumination of an air-free suspension. The postirradiation reaction continues for more than 20 min before the change in $[Cl^-]$ falls below the detection limit of the ISE.

Several additional experiments were conducted to probe the photochemical and postirradiation processes. An experiment similar to the one yielding the data of the inset in Figure 3 provided evidence that the postirradiation reaction was very sensitive to the presence of air. First, a degassed suspension irradiated for 3 min was kept in the dark for 40 s, followed by a brief introduction of air via briefly puncturing the septum seal. As expected, formation of both Cl^- and F^- declined once illumination stopped but then became negligible within one minute of introducing air into the suspension. This observation is in stark contrast with the findings obtained under continuous illumination where introduction of small amounts of O_2 actually enhanced the subsequent Cl^- photogeneration. Other experiments evaluated the influence of the CFC−aqueous interface on the chain reaction kinetics. The addition of more than 82 μL of CFC 11 resulted in a second liquid phase consisting of small droplets dispersed throughout the suspension by the action of stirring. TiO_2 suspensions containing only 80 μL of CCl_3F liquid exhibited a single aqueous phase, and illumination of such systems yielded the same two-stage process typical of systems containing 2.0 mL of CFC. However, unlike suspensions with excess liquid CFC, no postirradiation effect was detected when the amount of CCl_3F added was below the solubility limit. Instead, the CCl_3F photoreduction restarted immediately upon illumination after a dark period and $r(Cl^-)$ decreased as shown in Figures 2 and 3 for suspensions containing excess CFC.

The nonaqueous phase had a clear impact on the rate of CCl_3F photoreduction and yields of photogenerated Cl^-. Visual inspection showed that the TiO_2 powder remained suspended exclusively in the aqueous phase. An increasing number of liquid CFC droplets formed when further CCl_3F was added to stirred aqueous TiO_2 suspensions. The obvious consequence is an

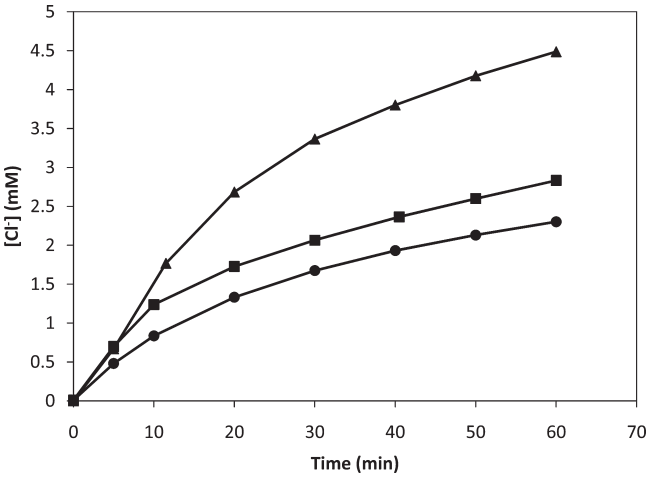

Figure 4. Plot of $[Cl^-]$ vs time for Ar-saturated suspensions containing 2.0 mL (▲), 1.0 mL (■), and 70 μL (●) of CFC 11 in the presence of 0.3 M HCO_2^-/HCO_2H buffer and 0.50 g L^{-1} of TiO_2 at pH 5.9 irradiated with 1.1×10^{-6} M $h\nu$ s^{-1}.

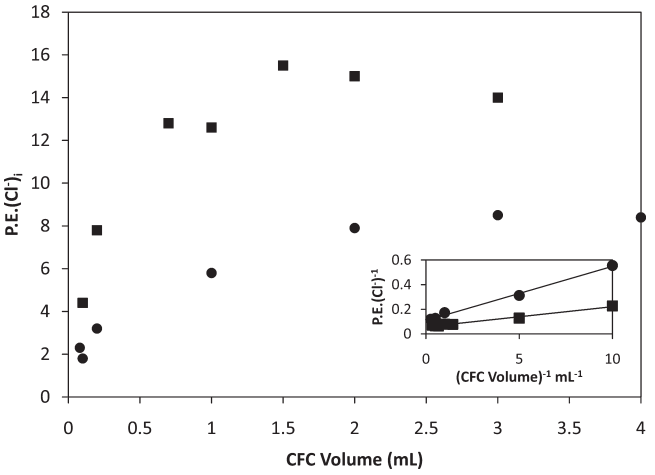

Figure 5. P.E.(Cl^-) vs CFC volume for Ar- (●) and air-saturated (■) suspensions containing 0.3 M HCO_2^-/HCO_2H buffer and 0.50 g L^{-1} of TiO_2 at pH 5.9 and irradiated with $I_o = 1.0 \times 10^{-6}$ M $h\nu$ s^{-1}. Inset shows the same data plotted as P.E.$(Cl^-)_i^{-1}$ vs $(\text{CFC volume})^{-1}$.

increase of the total surface area of the aqueous−CFC interface since the average diameter of the droplets appeared to remain constant. Figure 4 shows the changes in $[Cl^-]$ as a function of time for deaerated suspensions containing 70 μL and 1.0 and 2.0 mL of CFC 11. Chloride ions were photogenerated in all cases, but the yield of Cl^- doubled when 2.0 mL of CCl_3F were present. No further improvements in the Cl^- formation were detected upon further increasing of the amount of CFC added. Also, the $[Cl^-]$ produced during the induction periods was unaffected by the volume of CFC present. Air-saturated suspensions yielded results similar to those displayed in Figure 4, albeit they exhibited higher chloride yields and longer induction periods as was typical of such systems. Illustrated in Figure 5 is the variation of P.E.$(Cl^-)_i$ as a function of CCl_3F volume (V_{CFC}), which reached a maximum value at 1.5−2 mL and remained constant thereafter for both air-saturated and air-free suspensions. Presented in the inset of Figure 5 is a plot of P.E.$(Cl^-)_i^{-1}$ vs V_{CFC}^{-1}. Such double reciprocal plots resulted in

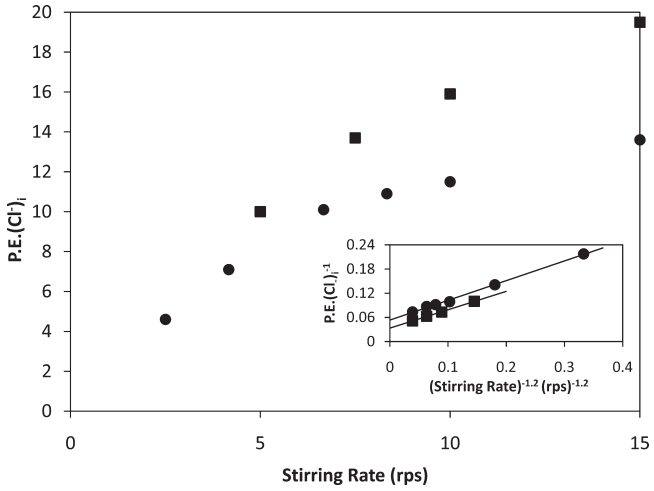

Figure 6. Effect of stirring rate on P.E.$(Cl^-)_i$ for air-free (●) and air-saturated (■) suspensions containing 2.0 mL of CFC 11, 0.3 M formate/formic acid buffer, and 0.50 g L^{-1} of TiO_2 at pH 5.9 irradiated with $I_o = 1.0 \times 10^{-6}$ M $h\nu$ s^{-1}. The inset illustrates the linear relationship between P.E.$(Cl^-)_i^{-1}$ and the stirring rate raised to the −1.2 power.

straight lines for both sets of data, but the results obtained from air-saturated systems exhibited a smaller slope.

Alterations of the interfacial surface area can also be accomplished by varying the stirring rate (N) while maintaining constant V_{CFC}. Rapid stirring of the suspensions causes larger CFC droplets to fragment forming additional droplets of smaller size. Variations in the stirring rate induced no changes in the characteristic features of photoreactions conducted in air-free or air-saturated suspensions such as the initial induction periods and subsequent fast steps of Cl^- photogeneration. However, as shown in Figure 6, changes in the stirring rate (N) influenced the rates of the photoreactions. Namely, increasing the stirring rate improved the efficiency of the CCl_3F photoreduction. Experiments with $N < 2.5$ rps were not feasible because the TiO_2 powder settled on the bottom of the reaction vessel under those conditions, which, in turn, exposed the reference electrode to UV light and generated artificial signals. Shown in the Figure 6 inset is a reciprocal plot depicting the linear relationship between P.E.$(Cl^-)_i^{-1}$ and the stirring rate raised to the −1.2 power for air-free and air-saturated suspensions. The slopes for the two linear trendlines are within 10% of each other and the *y*-intercepts are 0.053 and 0.033, respectively.

DISCUSSION

Previous studies showed that illumination of TiO_2 suspensions induced dehalogenation of CCl_3F forming $HCCl_2F$ and Cl^- as main products through a photoinitiated chain reaction.[10] Reducing species, e^-_{cb} and $\bullet CO_2^-$, form through UV excitation of electrons into the conduction band or oxidation of formate by photogenerated valence band holes,[18] respectively. They initiate a chain process by reducing CCl_3F on the surface of the TiO_2 particle and generating Cl^- and $\bullet CCl_2F$ radicals able to abstract hydrogen atoms from the formate buffer to yield $HCCl_2F$ and another $\bullet CO_2^-$ radical. Both $\bullet CCl_2F$ and $\bullet CO_2^-$ act as chain carriers, and their migration away from the oxide surface propagates the chain reaction into the solution. Chain termination occurs via a cross-reaction of the chain carriers forming a

carbine radical (:CClF) that subsequently decays via hydrolysis producing additional Cl^- ions and a F^- ion. The experimental observations obtained in air-free suspensions are consistent with the following mechanism:[10b]

$$TiO_2 + h\nu \rightarrow h^+_{vb} + e^-_{cb} \quad (2)$$

$$h^+_{vb} + e^-_{cb} \rightarrow \text{heat} \quad (3)$$

$$h^+_{vb} + H_2O \rightarrow OH\bullet + H^+ \quad (4)$$

$$h^+_{vb}/OH\bullet + HCO_2^- \rightarrow \bullet CO_2^- + H^+/H_2O \quad (5)$$

$$\bullet CO_2^- + TiO_2 \rightarrow e^-_{cb} + CO_2 \quad (6)$$

$$e^-_{cb} + CCl_3F \rightarrow \bullet CCl_2F + Cl^- \quad (7)$$

$$\bullet CO_2^- + CCl_3F \rightarrow \bullet CCl_2F + Cl^- + CO_2 \quad (8)$$

$$\bullet CCl_2F + HCO_2^- \rightarrow \bullet CO_2^- + HCCl_2F \quad (9)$$

$$\bullet CCl_2F + \bullet CO_2^- \rightarrow :CClF + Cl^- + CO_2 \quad (10)$$

$$\bullet CCl_2F + e^-_{cb} \rightarrow :CClF + Cl^- \quad (11)$$

$$:CClF + 2H_2O \rightarrow HCO_2^- + 3H^+ + Cl^- + F^- \quad (12)$$

Experiments performed with suspensions initially saturated with air yield a more efficient reductive chain dehalogenation of CCl_3F, which can be rationalized upon inclusion of the following additional steps:[10b]

$$2e^-_{cb} + O_2 + 2H^+ \rightarrow H_2O_2 \quad (13)$$

$$e^-_{cb} + H_2O_2 \rightarrow OH^- + OH\bullet \quad (14)$$

Reduction of O_2 by $\bullet CO_2^-$ also occurs

$$\bullet CO_2^- + O_2 \rightarrow O_2^- + CO_2 \quad (15)$$

but O_2^- is incapable of reducing CCl_3F as e^-_{cb} and $\bullet CO_2^-$ do in reactions 7 and 8. Thus, the induction periods noticed in curves A and B of Figure 1 result from the scavenging of e^-_{cb} and $\bullet CO_2^-$ by O_2, which inhibits reduction of CCl_3F via steps 7 and 8. Scavenging of the reducing species by traces of O_2 explains the much shorter induction periods observed in Ar-saturated suspensions. Transformation of O_2 into H_2O_2 is known to occur upon illumination of TiO_2 in the presence of air and HCO_2H.[20] After the induction period is completed, the resulting peroxide aids the conversion (via steps 14 and 5) of the weakly reducing e^-_{cb} into $\bullet CO_2^-$, which is a much stronger reductant.[6,13] Hence, the higher P.E.$(Cl^-)_i$ values shown in Figure 2 for air-saturated systems after most of the O_2 is consumed are a consequence of step 14 followed by step 5.[10a]

The results presented in curve C of Figure 1 are interesting since they confirm that formation of chloride during the induction period is a photoinitiated process given that no change in $[Cl^-]$ was detected during the dark periods. Another significant observation pertains to the much longer induction period noticed when intermittent illumination was applied throughout experiments performed with air-saturated suspensions. In fact, the induction period is not complete until after cumulative 39 min of illumination (in addition to 39 min in the dark), as compared to the 10−15 min of photolysis typically observed under continuous exposure to light. A process that may account for such an unusual observation is the thermal disproportionation of H_2O_2:[21]

$$2H_2O_2 \rightarrow H_2O + O_2 \quad (16)$$

which proceeds with $k_{16} = 3.9 \times 10^{-4}\ s^{-1}$ in the presence of TiO_2. Some of the O_2 converted into H_2O_2 is regenerated via step 16; the effect of this reaction would be most significant during the dark periods since oxygen is reduced under illumination via step 13. Occurrence of step 16 is a logical explanation for the results shown in curve C of Figure 1 given that reformation of O_2 during the dark periods is anticipated to extend the duration of the induction step. In addition, step 16 provides an explanation for the short induction period noticed during intermittent photolysis of suspensions initially saturated with air. Delayed Cl^- formation was only observed during the illumination part of a duty cycle and may originate from O_2 reformation in the preceding dark period. Regeneration of O_2 during illumination via reaction 16 could also explain the lower values of $[Cl^-]/[F^-]$ obtained in air-saturated suspensions as compared with the ratios determined in degassed systems.[10a] Formation of $\bullet O_2CCl_2F$ radicals is known to take place via[22]

$$\bullet CCl_2F + O_2 \rightarrow \bullet O_2CCl_2F \quad (17)$$

and an H-atom from HCO_2^- by the resulting peroxy radical is anticipated to form halide ions through the overall process

$$\bullet O_2CCl_2F + H_2O + HCO_2^- \rightarrow \bullet CO_2^- + 2Cl^- + F^- + \text{products} \quad (18)$$

Because the later transformation is not a termination step, occurrence of steps 17 and 18 yields amounts of F^- larger than those produced when only reactions 10 to 12 take place.

The results presented in Figures 1−3 clearly demonstrate that postirradiation reduction of CCl_3F takes place. These observations together with P.E.$(Cl^-) > 1$ and the large ratios of $[Cl^-]$ to $[F^-]$ obtained during illumination confirm that the reduction of CCl_3F initiated by photolysis of TiO_2 suspensions takes place via a chain process. Utilization of continuous or intermittent light exposures during the induction period had no effect on the subsequent chain photoreactions: P.E.(Cl^-) values for the experiments of curves B and C of Figure 1 were 13.7 and 13.3, respectively, and $[Cl^-]$ was 9.8 mM and 10.1 mM, respectively, after 30 min of illumination. However, the behavior of the postirradiation reactions is strongly influenced by the photolytic initiation process. The high $[Cl^-]/[F^-]$ determined during the postirradiation processes mimic those measured under continuous illuminations. Hence, the postirradiation processes are a continuation of the photoinitiated chain transformations. Interestingly, introduction of O_2 into an air-free system during a dark period caused the formation of Cl^- and F^- to stop quickly, whereas an enhanced chloride ion generation occurs upon introduction of oxygen under illumination. These observations indicate that reduction of O_2 to H_2O_2 consumes most of the chain carriers and that the resulting peroxide is no longer able to generate reductants in the absence of light.

As shown in Figure 2, both air-saturated and air-free systems experience post irradiation reactions, but the former are characterized by higher reaction rates in the presence and absence of light. These differences are likely due to the presence of small amounts of dissolved O_2 resulting from reaction 16, but other potential sources of oxygen are the CFC droplets. The persistent presence of a small amount of O_2 can induce a faster

production of chloride ions even after many light/dark cycles, as illustrated in Figure 2. The influence of small volumes of O_2 gas on the kinetic behavior of these systems has been demonstrated previously.[10a]

Optical experiments with P-25 powders containing H_2O have shown that photogenerated electrons can accumulate on the TiO_2 surface forming deeply trapped and persistent electrons that are fairly unreactive.[23] Formation of such trapped electrons seems plausible in the presence of formate ions because valence band holes are scavenged effectively through reaction 5 forming $\bullet CO_2^-$. This strong reducing agent can then react efficiently with CCl_3F even away from the semiconductor surface. Fast removal of holes leads to higher concentrations of surface and trapped electrons, which lowers the efficiency of chain initiation by increasing the rate of charge carrier recombination.[14] An enhanced carrier recombination is the most probable cause for the gradual decrease of $r(Cl^-)$ during illumination illustrated in curve A of Figure 1 and in Figure 4.

The inset of Figure 3 shows that when illumination of an air-free TiO_2 suspension is terminated, the postirradiation process continues for over 20 min until all chain carriers are consumed. Figures 2 and 3 show that initial P.E.(Cl^-) values remained constant for the first two cycles when the dark period amounts to 27 min. In contrast, lower P.E.(Cl^-) values are obtained from cycle 2 onward for systems undergoing dark periods between 17 and 0.5 min. Cycles with dark periods of 17 min or less yielded P.E.(Cl^-) values similar to those obtained during continuous illumination for the same total length of time. This means that not only maximum P.E.(Cl^-) values can be obtained after complete removal of the trapped electrons but also that injection of some electrons into the oxide particles via step 5 takes place in the dark. Hence, efficient chain reactions occur exclusively on TiO_2 surfaces that are free of charge carriers, similar to the surface environment existing at the beginning of the photolysis. As shown in Figure 3, P.E.(Cl^-) values obtained for the longest dark period also decline after two light/dark cycles probably due to other factors that could inhibit the chain initiation, such as the adsorption of Cl^- on reactive TiO_2 surface sites.[24]

While the suspension pH has a significant effect on the rate and amount of chloride formed in the photoinitiated reaction, identical amounts of chloride ions formed during dark periods of reactions regardless of the solution $[H^+]$. The effect of low pH during illumination is due to two factors. First, the presence of formic acid ($pK_a = 3.75$) on the TiO_2 surface, instead of formate ions, slows the formation of chain initiators via step 5. Also, the reduction potential of e^-_{cb} decrease as $[H^+]$ increases, making reaction step 6 less favorable.[13] No initiation occurs during dark periods, and therefore, chain propagation is independent of pH. This is consistent with the proposed mechanism for the photochemical CCl_3F dehalogenation described previously in which $\bullet CO_2^-$, rather than e^-_{cb}, is involved in propagating the reaction away from the TiO_2 surface.

Figures 4 and 5 demonstrate that excess CFC is necessary to observe several of the interesting features of this system including selective $HCCl_2F$ formation, P.E.$(Cl^-)_i > 2$, and postirradiation reactions. Figure 4 shows that larger yields of $[Cl^-]$ photogeneration are obtained for systems containing excess CFC (more than 80 μL of CCl_3F liquid added). Reactions between species present in different liquid phases often follow complex rate laws since the reaction rates depend on the interfacial surface area.[25] The kinetics of such processes can be described in terms of a thin diffusion film existing between the aqueous and organic phases. In this model, the concentration of the organic solute in the aqueous phase is controlled by the combined effect of the diffusion speed through the layer and the rate of consumption of this compound in aqueous solution. For moderately fast aqueous reactions, a concentration gradient of organic material (CCl_3F) is established across the film. The concentration of CCl_3F in the aqueous phase is less than the solubility limit because the reaction occurs to some extent within the interfacial region. Since the data of Figure 5 indicates that Cl^- forms via a chain process at all CFC volumes, a logical assumption is that CFC consumption and Cl^- generation are related mainly through the second-order reaction 8. This assumption results in $-r(CFC) = r(Cl^-)$, with $-r(CFC)$ expressing the rate of CFC consumption. A general solution for second-order reactions occurring in a two-phase liquid system is known,[26] which in the CFC system yields

$$r(Cl^-)_i = \frac{k_{aq/org} SA n k_8 [CFC]_{sat} [\bullet CO_2^-]_{ss}}{k_{aq/org} SA n + k_8 [\bullet CO_2^-]_{ss}} \quad (19)$$

where $k_{aq/org}$ is the mass transfer coefficient or rate constant for the solute transport from organic to aqueous phase, $[CFC]_{sat}$ is the solubility limit of CCl_3F in water (8.1×10^{-3} M), $[\bullet CO_2^-]_{ss}$ is the steady-state concentration of carboxyl radicals in the aqueous phase, SA is the surface area of an individual droplet per unit volume of aqueous solution, and n is the number of droplets. Hence, when a large excess of CCl_3F is added, such as in the experiments with 2.0 mL of CCl_3F, SAn is very large and $k_{aq/org} SA n \gg k_8 [\bullet CO_2^-]_{ss}$, reducing eq 19 to the previously proposed rate law[10b] shown in eq 20.

$$r(Cl^-)_i = k_8 [CFC]_{sat} [\bullet CO_2^-]_{ss} \quad (20)$$

Occurrence of a moderately fast reaction in the aqueous phase is consistent with the limiting P.E.$(Cl^-)_i$ at high CFC volume, which is a typical characteristic of such two-phase systems.

Inverting both sides of eq 19 and multiplying by I_o yields eq 21.

$$\frac{1}{\text{P.E.}(Cl^-)_i} = \frac{I_o}{k_8 [CFC]_{sat} [\bullet CO_2^-]_{ss}} + \frac{I_o}{k_{aq/org} [CFC]_{sat} SA n} \quad (21)$$

Addition of more CFC to a stirred suspension is assumed to create additional spherical droplets of the same size. Although the interfacial surface area is unknown because the average CFC droplet size has not been measured, the surface area of a droplet can be related to the CFC volume by the geometric formula $SA = 3V_{CFC}(nR)^{-1}$, where R is the average radius of the CFC droplets. Substituting this relationship for surface area into eq 21 yields the following equation that relates P.E.$(Cl^-)_i^{-1}$ with V_{CFC}^{-1}:

$$\frac{1}{\text{P.E.}(Cl^-)_i} = \frac{I_o}{k_8 [CFC]_{sat} [\bullet CO_2^-]_{ss}} + \frac{nRI_o}{3k_{aq/org} [CFC]_{sat} V_{CFC}} \quad (22)$$

The inset of Figure 5 demonstrates that eq 22 is consistent with the results gained in the TiO_2 suspensions. The reciprocal of the y-intercept can be interpreted as P.E.$(Cl^-)_i$ measured in a suspension using CCl_3F as the solvent, if such a reaction was possible. For air-free and air-saturated suspensions, maximum P.E.$(Cl^-)_i$ values calculated from the y-intercepts are 9.3 and 17.2, respectively. These values agree with the average P.E.$(Cl^-)_i$ measured with 2.0 mL of CFC in each system (7.9 and 15, respectively) within experimental error. Since the y-intercept predicts a value of P.E.$(Cl^-)_i$ for a system containing only liquid

CFC, this agreement with the experimental data indicates that an excess amount is already present in suspensions containing 2.0 mL. A similar conclusion can be drawn from Figure 5 by noting that the values of P.E.$(Cl^-)_i$ remain constant for both air- and Ar-saturated suspensions containing more than 1.5−2 mL of CFC. Different intercepts are obtained for reactions with and without air because, according to eq 22, the denominator of the first term on the right side depends on $[\bullet CO_2^-]_{ss}$. Previous studies of this system have established that the concentration of $\bullet CO_2^-$ differs greatly between aerated and deaerated suspensions.[10] The concentration of carboxyl radical anions is higher in aerated suspensions due to the consumption of O_2 through reactions 17 and 18. Since $[\bullet CO_2^-]$ is larger in suspensions with air as compared with their air-free counterparts, a smaller intercept is obtained for the former systems. It is assumed that the values of other factors appearing in the first term of eq 22, i.e., k_8, $[CFC]_{sat}$, and I_o, are constant regardless of the presence of air or argon gas in the reactor headspace.

An empirical relationship has been proposed that relates the surface area of an organic liquid dispersed in an aqueous solution as inversely proportional to N, the stirring rate, raised to the 1.2 power.[27] Using this relationship, eq 22 can be modified to show that P.E.$(Cl^-)_i^{-1}$ is linearly dependent upon $N^{-1.2}$ according to eq 23.

$$\frac{1}{\text{P.E.}(Cl^-)_i} = \frac{I_o}{k_8[CFC]_{sat}[\bullet CO_2^-]_{ss}} + \frac{nRI_o}{3k_N k_{aq/org}[CFC]_{sat}N^{1.2}} \quad (23)$$

where k_N is the proportionality constant relating the droplet radius to $N^{-1.2}$. The inset of Figure 6 shows that the data sets for deaerated and aerated systems have similar slopes but that the maximum P.E.$(Cl^-)_i$ values are 19 and 30, respectively. Slopes of the best fit lines are expected to be equal for both systems since the light intensity and their initial compositions are the same. The y-intercept for data collected from an air saturated solution is lower due to the higher concentration of radical intermediates present at the beginning of the reaction's second stage. Air saturated suspensions have higher maximum photonic efficiencies due to a greater concentration of $\bullet CO_2^-$, as is the case for the inset of Figure 5. Both maximum P.E.$(Cl^-)_i$ values are twice as large as is observed under typical experimental conditions. This is due to rapid stirring, which ensures that reaction products move away from the interface quickly, allowing more aqueous reactants to approach the CFC droplet. Higher reaction rates result because of the increased interaction between $\bullet CO_2^-$ and $CCl_3F_{(l)}$. Another explanation may be considered. If a suspension was to be stirred fast enough, the CFC droplets would become very small, and the organic phase would become completely soluble under such conditions, making all CCl_3F molecules available to react with other species in solution. However, this is simply another way of describing the scenario presented to explain the results of the Figure 5 inset. In that case, the largest possible excess of CFC liquid yielded P.E.$(Cl^-)_i$ values that were only slightly higher than those recorded for suspensions containing 2.0 mL of CFC. Therefore, rapid diffusion of products away from the CFC liquid surface is an additional factor that can increase the photonic efficiency of the chain reaction.

CONCLUSIONS

Studies of the influence of periodic exposure to UV light have revealed details of why oxygen alters the photocatalyzed chain reduction of CCl_3F to $HCCl_2F$ and Cl^- during the induction period and chain propagation steps. Results are consistent with previous studies of this system and extend the understanding of how the chain reaction propagates away from the catalyst surface in the absence of light. Varying the stirring rate and the volume of CFC liquid show that the surface area between the aqueous and CCl_3F phases and diffusion of products away from that interface play a significant role in the efficiency of the reduction process.

AUTHOR INFORMATION

Corresponding Author

*E-mail: kwinkel@fit.edu (K.W.); millsge@auburn.edu (G.M.).

Present Addresses

§Chemistry Department, U.S. Naval Academy, Annapolis, Maryland 21402, United States.

ACKNOWLEDGMENT

We thank Degussa/Evonic for donating the P-25 TiO_2 material, the U.S. Navy CIVINS program for supporting R.L. C., and NTC for partial funding of this research.

REFERENCES

(1) De Richter, R.; Caillol, S. *J. Photochem. Photobiol., C* **2011**, *12*, 1–19.

(2) (a) Mills, A.; Le Hunte, G. *J. Photochem. Photobiol., A* **1997**, *108*, 1–35. (b) Hoffmann, M. R.; Martin, S. T.; Choi, W.; Bahnemann, D. W. *Chem. Rev.* **1995**, *95*, 69–96.

(3) (a) Micic, O. I.; Zhang, Y.; Cromak, K. R.; Trifunac, A. D.; Thurnauer, M. C. *J. Phys. Chem.* **1993**, *97*, 7277–7283. (b) Grela, M. A.; Coronel, M. E. J.; Colussi, A. J. *J. Phys. Chem.* **1996**, *100*, 16940–16946.

(4) (a) Neumann, A.; Hofstetter, T. B.; Skarpeli-Liati, M.; Schwarzenbach, R. P. *Environ. Sci. Technol.* **2009**, *43*, 4082–4089. (b) Pecher, K.; Haderlein, S. B.; Schwarzenbach, R. P. *Environ. Sci. Technol.* **2002**, *36*, 1734–1741.

(5) (a) Huston, P. L.; Pignatello, J. J. *Environ. Sci. Technol.* **1996**, *30*, 3457–3463. (b) Hu, C.-M.; Tu, M.-H. *J. Fluorine Chem.* **1991**, *55*, 105–107. (c) Bullock, G.; Cooper, R. *Trans. Faraday Soc.* **1970**, *66*, 2055–2064.

(6) Stanbury, D. M. *Adv. Inorg. Chem.* **1989**, *33*, 69–138.

(7) Solomon, S. *Rev. Geophys.* **1999**, *37*, 275–316.

(8) (a) Powell, R. L. *J. Fluorine Chem.* **2002**, *114*, 237–250. (b) Wallington, T. J.; Schneider, W. F.; Worsnop, D. R.; Nielsen, O. J.; Sehested, J.; Debruyn, W. J.; Shorter, J. A. *Environ. Sci. Technol.* **1994**, *28*, 320A–326A.

(9) Weaver, S.; Mills, G. *J. Phys. Chem.* **1997**, *101*, 3769–3775.

(10) (a) Winkelmann, K.; Calhoun, R. L.; Mills, G. *J. Phys. Chem. A* **2006**, *110*, 13827–13835. (b) Calhoun, R. L.; Winkelmann, K.; Mills, G. *J. Phys. Chem. B* **2001**, *105*, 9739–9746.

(11) (a) Stark, J.; Rabani, J. *J. Phys. Chem. B* **1999**, *103*, 8524. (b) Choi, W.; Hoffmann, M. R. *Environ. Sci. Technol.* **1997**, *31*, 89–95.

(12) Cornu, C. J. G.; Colussi, A. J.; Hoffmann, M. R. *J. Phys. Chem. B* **2001**, *105*, 1351–1354.

(13) Ward, M. D.; White, J. R.; Bard, A. J. *J. Am. Chem. Soc.* **1983**, *105*, 27–31.

(14) Gerischer, H.; Heller, A. *J. Phys. Chem.* **1991**, *95*, 5261–5267.

(15) Horvath, A. L. *Halogenated Hydrocarbons: Solubility-Miscibility with Water*; Marcel Dekker: New York, 1982; pp 661−663.

(16) Heller, H. G.; Langan, J. R. *J. Chem. Soc., Perkin Trans.* **1981**, *2*, 341–343.

(17) Salinaro, A.; Emeline, A. V.; Zhao, J.; Hidaka, H.; Ryabchuk, V. K.; Serpone, N. *Pure Appl. Chem.* **1999**, *71*, 321–335.

(18) Perissinotti, L. L.; Brusa, M. A.; Grela, M. A. *Langmuir* **2001**, *17*, 8422–8427.

(19) Brault, D.; Neta, P. *J. Phys. Chem.* **1983**, *87*, 3320–3327.

(20) Shiraishi, F.; Nakasako, T.; Hua, Z. *J. Phys. Chem. A* **2003**, *107*, 11072–11081.
(21) Hiroki, A.; LaVerne, J. A. *J. Phys. Chem. B* **2005**, *109*, 3364–3370.
(22) Alfassi, Z. B.; Mosseri, S.; Neta, P. *J. Phys. Chem.* **1987**, *91*, 3383.
(23) Szczepankiewicz, S. H.; Colussi, A. J.; Hoffmann, M. R. *J. Phys. Chem. B* **2000**, *104*, 9842–9850.
(24) Abdullah, M.; Low, G. K.; Matthews, R. W. *J. Phys. Chem.* **1990**, *94*, 6820–6825.
(25) Cox, B. G. *Modern Liquid Phase Kinetics*; Oxford Press: New York, 1994; Vol. 21, Chapter 6.
(26) Doraiswamy, L. K.; Sharma, M. M. *Heterogeneous Reactions: Analysis, Examples and Reactor Design*; Wiley-Interscience: New York, 1984; Vol. 2, Chapter 3.
(27) McDonough, R. J. *Mixing for the Process Industries*; Van Nostrand Reinhold: New York, 1992; p 192.